JOURNAL OF MODERN OPTICS, 10 NOVEMBER–15 DECEMBER 2004
VOL. 51, NO. 16–18, 2771–2780

Taylor & Francis
Taylor & Francis Group

Ultrafast optical and magneto-optical studies of III–V ferromagnetic semiconductors

J. WANG†, G. A. KHODAPARAST†, J. KONO†*,
A. OIWA‡ and H. MUNEKATA‡

†Department of Electrical and Computer Engineering, Rice Quantum Institute, and Center for Nanoscale Science and Technology, Rice University, Houston, Texas 77005, USA
‡Imaging Science and Engineering Laboratory, Tokyo Institute of Technology, Yokohama, Kanagawa 226-8503, Japan

(*Received 15 February 2004*)

Abstract. We use ultrafast optical techniques to investigate the dynamics of charge and spin carriers and coherent phonons as well as magnetic order in III–V ferromagnetic semiconductors. We observe a rich array of dynamical phenomena that are absent in traditional nonmagnetic semiconductors or metallic ferromagnets. Very short charge and spin lifetimes of the photoinjected carriers (~2 ps) and multi-level charge decay dynamics are observed, which are attributed to a large density of mid-bandgap states introduced during low temperature molecular beam epitaxy (LT-MBE) growth and highly *p*-type Mn doping. During the very short free carrier lifetime, the coercivity of the system is seen to be reduced. We attribute this photo-induced 'softening' to the transient modification of carrier-mediated ferromagnetic exchange coupling between Mn spins. After the photogenerated free electrons are trapped by defects, periodic oscillations appear in differential reflectivity due to the coherent generation of acoustic phonon wavepackets.

1. Introduction

Recently, there have been various innovative experimental studies on the dynamics of strongly-correlated electron systems, especially with macroscopic order (e.g. photoinjected carriers in metallic ferromagnets and nonequilibrium quasi-particles in the high-T_c cuprates) [1–4]. One of the common themes of these studies is to understand how ultrafast laser pulses can alter an ordered phase through many-body and strong correlation effects in a sea of interacting carriers. In particular, the demonstrations of femtosecond demagnetization in ferromagnetic metals indicate that transient carriers excited by ultrashort laser pulses can effectively modify collective magnetic order in an ultrafast regime, sometimes even within the laser pulse width [4]. Until now, such investigations have been mainly limited to metallic systems, in which thermal effects are commonly believed to dominate the dynamical processes. The microscopic understanding of effective energy transfer channels among the subsystems (charge, spin and lattice) before the heating of the phonons is still elusive.

*Author for correspondence. e-mail: kono@rice.edu

Journal of Modern Optics ISSN 0950–0340 print/ISSN 1362–3044 online
http://www.tandf.co.uk/journals
DOI: 10.1080/09500340412331284948

III–V dilute magnetic semiconductors (DMSs) [5, 6] provide another model system to probe a variety of novel magneto-optical processes. In III–V DMSs, the strong *p–d exchange interaction* between mobile carriers (i.e. holes) and the embedded magnetic moments stabilizes ferromagnetic order at low temperatures. This Mn–Mn exchange interaction is sensitive to the carrier density and is expected to be strongly modified by a large density of spin-coherent carriers upon optical excitation. In addition, transient optical spectroscopy provides an ideal means for studying some of the unique properties of III–V DMSs, such as the existence of a large density of mid-bandgap states and heavy *p*-doping, as these will seriously influence the dynamical response of semiconductors [7]. However, there have been few ultrafast optical measurements on III–V DMSs to clarify the importance of low-temperature molecular beam epitaxy (LT-MBE) growth, and most current understanding is gleaned from static magnetization and electrical transport measurements. The need for experimental data is also fuelled by a growing interest in semiconductor spintronics, which promise future 'multifunctional' devices capable of information processing, storage, and communications in a single device. The recent demonstrations of voltage-tuned [8] and photoinduced [9] alteration of carrier-induced ferromagnetism in the model III–V DMS InMnAs have provided a prototype for such device concepts.

Here we report ultrafast optical and magneto-optical studies of ferromagnetic InMnAs and InGaMnAs. We have developed a two-colour method of time-resolved magneto-optical Kerr effect (TR-MOKE) and transient reflectivity, which allows us to capture the dynamics of charge carriers, spins, and ferromagnetic order simultaneously. Ultrashort charge and spin lifetimes ($\sim$2 ps) and multi-level carrier decay dynamics are observed, which are attributed to a large density of bound states introduced during the LT-MBE growth and the highly *p*-type nature due to Mn doping. We observed *ultrafast photo-induced softening* (i.e. a transient decrease of coercivity) in a single InMnAs/GaSb heterostructure, which represents one of the first examples of femtosecond control of ferromagnetic order in semiconductors. Photogenerated transient carriers significantly *decrease* the coercivity (H_c) while sustaining the saturation magnetization. This transient softening persists only during the carrier lifetime ($\sim$2 ps) and returns to its original value as soon as the carriers recombine to disappear. After the photogenerated free electrons are trapped by defects, periodic oscillations appear in differential reflectivity due to the coherent generation of acoustic phonon wavepackets.

2. Experimental details

In order to separate various nonlinear effects and extract the genuine information on the dynamical response of III–V DMSs, we exploited a two-colour selective pumping scheme [10]. A 140 fs, midinfrared (MIR) 2 μm (1.26 μm) pump beam from an optical parametric amplifier (OPA) was used to create carriers only near the band edge of InMnAs (InGaMnAs) with 0.2 eV (0.1 eV) extra kinetic energy. This minimized the effects from the buffer layer and some purely nonlinear optical response, such as inter- or intra-valley scattering. A near-infrared (NIR) (775 nm) probe beam from a chirped pulse amplifier (Model CPA-2010, Clark-MXR, Inc.) allowed us to probe the energy

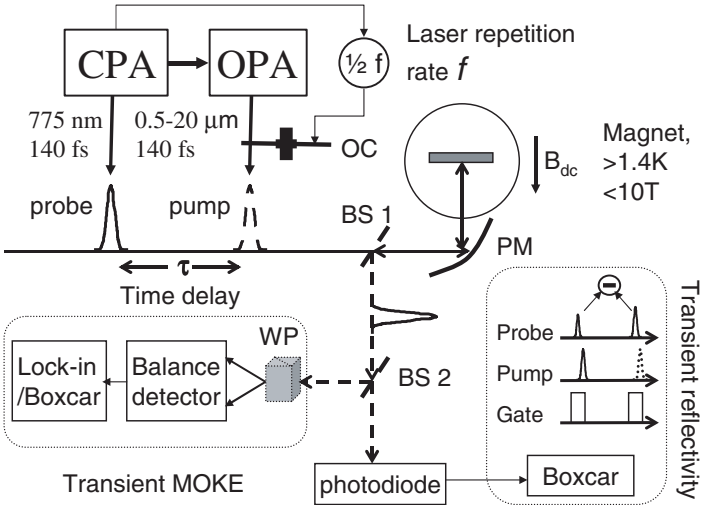

Figure 1. A schematic diagram of the experimental setup and data acquisition scheme. A small fraction ($\sim 10^{-5}$) of the chirped pulse amplifier (CPA) beam is used as a probe and the optical parametric amplifier (OPA) beam, tuned to 2 or 1.26 μm, is used as the pump. OC: optical chopper; BS: beam splitter; PM: parabolic mirror; WP: wollaston prism. Using this setup, we were able to record transient MOKE signal and transient reflectivity, simultaneously. See text for details.

levels far above the quasi-Fermi level of the optically excited carriers, which makes our data less susceptible to some carrier effects such as band filling (BF) and band gap renormalization (BGR).

The setup is detailed in figure 1. The probe beam and pump beam were made collinear by a non-polarizing beam splitter and then focused onto the sample mounted inside a superconducting magnet. We monitored transient MOKE signals by recording the intensity difference of the *s*- and *p*-components of the reflected NIR beam using a balanced detector, which were fed into a lock-in amplifier or a boxcar integrator. We monitored the transient reflectivity change by recording the intensity difference between adjacent reflected NIR pulses as a function of time delay while the pump was modulated by an optical chopper with a half harmonic of the laser repetition rate (500 Hz). Using a low repetition-rate laser (50 Hz–1 kHz) with a short pulse width (~150 fs) allowed us to probe the regimes of low average power (minimum thermal effect) and high peak fluence (maximum transient carrier density). This differentiates our study from previous time-domain magneto-optical studies [1, 4]. Under our pumping conditions, the maximum density of photocreated carriers was estimated to be comparable to or larger than the background carrier density ($\sim 10^{19}$ cm^{-3}), and, hence, significant modifications in exchange interactions can be expected.

The main Mn-doped samples studied were an InMnAs/GaSb single heterostructure and an InGaMnAs thin film, having the highest Curie temperature among each type ($T_c = 55$ K for InMnAs and $T_c = 110$ K for InGaMnAs). The samples were grown by LT-MBE. Detailed growth conditions and sample information were described previously [10, 11].

3. Experimental results

3.1. *Carrier charge dynamics*

Typical data showing ultrafast carrier dynamics in III–V magnetic semiconductors are presented in figures 2 (*a*) and (*b*). Similar multi-level carrier decay dynamics is observed in both InMnAs and InGaMnAs. First, the initial change in the differential reflectivity is negative for times less than 2 ps after photoexcitation (inset of figure 2). Second, a rapid rise is observed in reflectivity, leading to a sign change. Next, reflectivity oscillations with a period of ∼23 ps are observed. Finally, the signal shows a very slow decay to unity (several hundred ps).

In the case of a reference low-temperature InGaAs (LT-InGaAs) sample [figure 3 (*a*)], we observed a similar initial negative change in reflectivity and a subsequent fast rise with a sign change. On the other hand, in a high-temperature InGaAs (HT-InGaAs) sample [figure 3 (*b*)], the reflectivity change only showed a single exponential decay with a decay time of ∼104 ps. These facts led us to conclude that the fast (∼2 ps) decay of the initial negative signal, observed only in III–V DMSs and LT-InGaAs, reflects a unique feature of LT-MBE growth and can be attributed to the ultrafast trapping of electrons (by As_{Ga} antisite defects) and holes (by Ga vacancies), i.e. by mid-bandgap states due to defects. However, no clear oscillations were observed in LT-InGaAs. Instead, an 'overshoot' exists right after the sign change and before the very slow recovery starts.

3.2. *Carrier spin dynamics*

Circularly polarized pump beams can create spin-coherent carriers in DMSs via selection rules for interband transitions. Temporal profiles of femtosecond-resolved MOKE data are shown in figure 4. The two traces represent the photo-induced MOKE (PI-MOKE) signal versus time delay taken under the excitation by intense MIR radiation with two opposite senses of circular polarization, i.e. σ^+ and σ^-. An ultrafast photoinduced response, with pulse-width limited rising, is clearly evident in both cases and opposite circular polarizations result in *opposite*

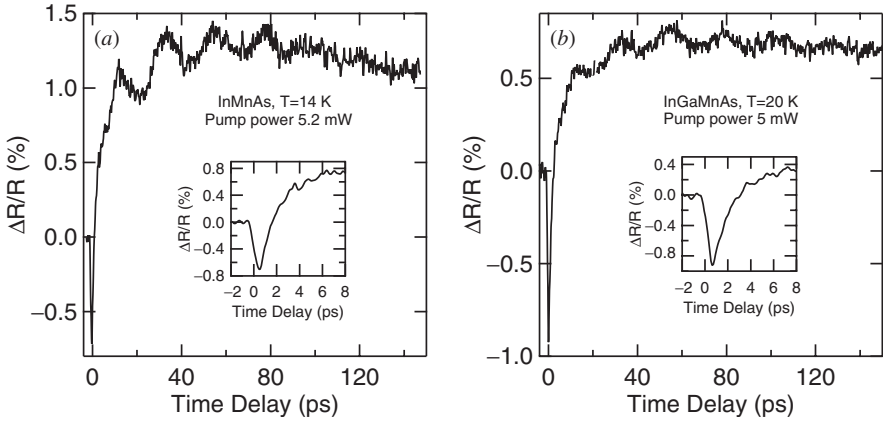

Figure 2. Differential reflectivity of InMnAs (*a*) and InGaMnAs (*b*), respectively. Insets: initial decay of ultrafast transients for InMnAs and InGaMnAs. The initial change in reflectivity is negative for times less than 2 ps. A fast bi-exponential rise follows, accompanied by oscillations with a period ∼23 ps. Finally, the signal shows a slow decay of several hundred ps.

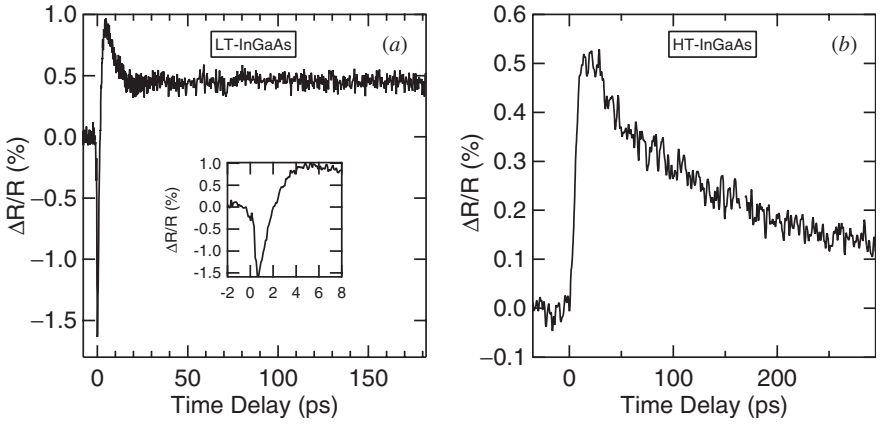

Figure 3. Differential reflectivity of LT-InGaAs (*a*) and HT-InGaAs (*b*) at 20 K, respectively. The experimental conditions are the same as the ones of figure 2 (*b*). Inset (left panel): initial decay of ultrafast transients for LT-InGaAs. A similar initial fast reduction and quick sign change in reflectivity is observed in LT-InGaAs, but not in HT-InGaAs.

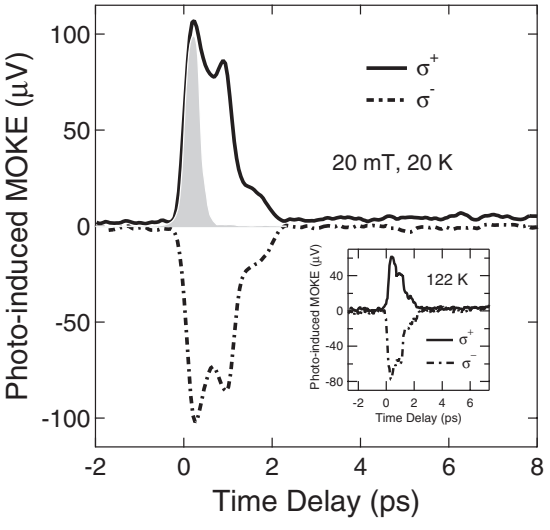

Figure 4. Photo-induced MOKE (PI-MOKE) of InMnAs at a temperature of 20 K versus time delay under pumping with circularly polarized 2-μm radiation, σ^- and σ^+. The shaded area is the pump-probe cross-correlation. Inset: PI-MOKE signal at 122 K.

signs and *symmetric shapes* of the PI-MOKE signal. In addition, we did similar measurements at elevated temperatures, including temperatures above the Curie temperature (55 K). As an example, data taken at 122 K are shown in the inset of figure 4. Here, we observed a similar ultrafast MOKE response as the ones at low temperatures. These facts clearly indicate that the temporal profiles of the PI-MOKE signals are most likely due to the relaxation of the spin polarization of the photoinjected carriers.

3.3. *Ultrafast photoinduced softening*

Figure 5 presents a detailed time evolution of ferromagnetic hysteresis loops in InMnAs at 20 K, demonstrating femtosecond optical softening. Ferromagnetic loops at fixed time delays are plotted in figures 5 (*a*) to (*h*). The data at negative time delays [figures 5 (*a*), (*b*)] show hysteresis loops with a finite coercivity. However, at a time delay of 450 fs [figures 5 (*c*), (*d*)], the hysteresis loops are totally suppressed in the horizontal direction, i.e. the coercivity is almost zero. Note that the ferromagnetic hysteresis loops shift to opposite directions under different pumping conditions, σ^+ and σ^-. The magnetic hysteresis loops continue to evolve and the softening lasts within the free carrier lifetime (~2 ps) [figures 5 (*e*) and (*f*)]. After this short amount of time, loops with the original H_c are recovered [figures 5 (*g*) and 5 (*h*)]. A more detailed examination indicates that almost no change is observed in the vertical height of the loop within the sensitivity of our setup. These facts lead us to conclude that lattice heating cannot be the reason for the above observations since raising the lattice temperature should result in loop shrinkage both horizontally and vertically. It is also worth mentioning that our pump power dependent measurements indicate that the fluence determines the degree of collapse, not the average power, which further points to a non-thermal origin of the observed phenomenon.

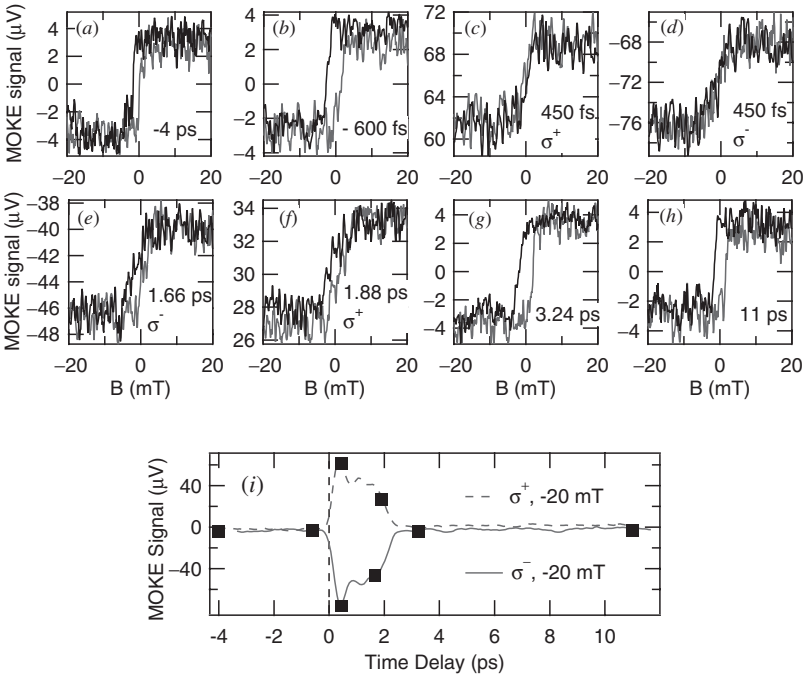

Figure 5. Ultrafast photo-induced softening in InMnAs. (*a*)–(*h*): MOKE signals against field at different time delays under pumping with circularly polarized 2-μm radiation. (*a*) −4 ps; (*b*) −600 fs; (*c*) 450 fs, pump was circularly polarized (σ^+); (*d*) 450 fs, σ^- ; (*e*) 1.66 ps, σ^-; (*f*) 1.88 ps, σ^+; (*g*) 3.24 ps; (*h*) 11 ps. A ferromagnetic hysteresis loop with finite coercivity is clearly seen in (*a*) and (*b*). In (*c*) and (*d*), the loop is nearly destroyed in the horizontal direction, i.e. coercivity is almost zero. (*i*): the vertical shifts of the magnetic loops against time delays follow the temporal profile of the MOKE signals.

4. Discussion

Let us first focus on the multi-level carrier dynamics in InMnAs and InGaMnAs. First, we attribute the initial pump-induced decrease in reflectivity to the decrease of the Drude dielectric constant due to intraband free carrier absorption (FCA). We can exclude any other free carrier effects, such as band gap renormalization (BGR) and band filling (BF), based on the following arguments. A simple estimation based on dielectric theory shows that BF results in a positive change in reflectivity at our probe wavelength (775 nm), so BF can be excluded. In the case of BGR, the change in refractive index is largest near the band edge and decreases rapidly with increasing probe photon energy. Thus, it should be substantially reduced at our probe wavelength, which is away from the band edge. Moreover, in III–V DMSs, band edge absorption is usually large but significantly smeared out by a large density of near band edge states introduced by defects [12]. This will drastically reduce the importance of BGR (and BF). Therefore, we conclude that the FCA mechanism is the dominant origin of the initial decrease in reflectivity.

Second, we ascribe the rapid rise of reflectivity that follows the initial decrease to a quick disappearance of photoinjected free carriers through ultrafast trapping by mid-gap states. This type of dynamics is commonly seen in low-temperature-grown III–V semiconductors. However, upon close examination of the rising processes of the III-Mn-V semiconductors and the LT-InGaAs reference sample, we notice subtle differences between the two. In III–V DMSs, a non-single exponential rising process is observed with periodic oscillations, which can be seen better in figures 6 (*a*) and 6 (*b*), where we plotted the rising components for InMnAs and InGaMnAs on log scale. A bi-exponential curve fitting yields decay times of 2 ps and 30 ps for InMnAs, 2 ps and 23 ps for InGaMnAs, respectively. In LT-InGaAs, on the other hand, the data show a single exponential rise with a decay time of ∼2 ps. Since the present III–V DMSs are highly *p*-type, it would be a reasonable speculation to attribute these differences to the different trapping rates for electrons and holes. Namely, we tentatively ascribe the fast component (which is also seen in LT-InGaAs) to electron trapping and the slow component (which is seen only in InGaMnAs and InMnAs) to hole trapping.

It should be noted that the temporal profiles of PI-MOKE measurements provide a direct measure of the spin lifetime of photogenerated carrier, which is ∼2 ps and similar to the charge lifetime. This indicates no spin conservation in the process of carrier trapping, which can be understood based on the Elliot–Yafet (E–Y) mechanism of spin relaxation [13]. Specifically, the strong spin-orbit coupling and interband mixing in narrow gap semiconductors, like InMnAs, manifest themselves in the spin dynamics during the carrier trapping process.

Third, the final decay process after the rising in reflectivity suggests slow recombination of the trapped carriers, which finally vacates the carrier traps. We should also notice that the final decaying process of LT-InGaAs is remarkably different from III–V DMSs (figures 2 and 3). The quick decay of the positive signal in LT-InGaAs (∼5 ps) suggests the existence of fast carrier depletion from the traps after initial trapping. Considering the nature of defects and current experimental conditions, we argue that the recombination mechanism is very different between LT-InGaAs and (III, Mn)Vs. We recall that in As-based LT semiconductors a small fraction of the charge neutral As_{Ga} is ionized to As^{+}_{Ga}, which acts as electron traps and is most likely to be saturated under current

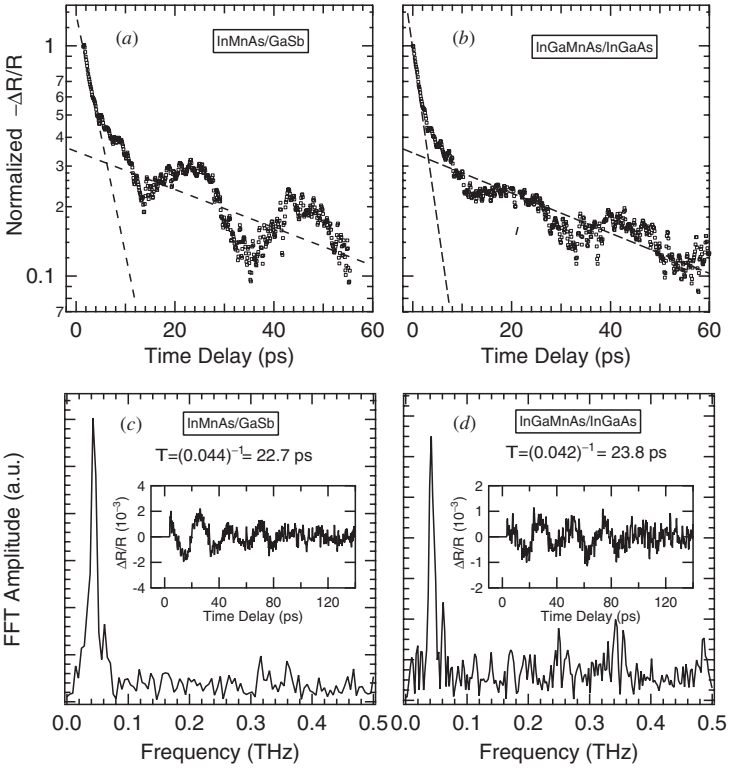

Figure 6. The fast-rising componets after initial negative transients in reflectivity of InMnAs (*a*) and InGaMnAs (*b*) are plotted on log scale. In magnetic semiconductors, a bi-exponential rising process, accompanied with periodic oscillations, was observed, while, in reference sample LT-InGaAs, a single exponential rise is seen. (*c*)–(*d*): the Fourier transforms of the oscillatory parts of the transient reflectivity signal in InMnAs and InGaMnAs (shown as insets), respectively.

pumping conditions. In (III, Mn)Vs, on the other hand, high acceptor-doping greatly lowers the Fermi energy and increases the concentration of As^{+}_{Ga}, which are not easy to saturate. Therefore, we expect that the final decay process in LT-InGaAs is faster than that in (III, Mn)Vs. This corroborates a complex and critical interplay between the mid-gap states and Mn-doping in carrier relaxation dynamics in III–V DMSs.

Next, let us discuss those periodic oscillations, which appear only in the magnetic samples [figures 6 (*c*)–(*d*)]. We believe that these oscillations are associated with coherent acoustic phonon wavepackets that are generated in the magnetic layer and propagate into the buffer layer. We further illustrate the detailed generation mechanism, using InMnAs/GaSb as an example. The pump pulse creates carriers only in the magnetic layer, where a large built-in electric field exists due to heavy Mn doping, surface Fermi energy pinning, and the type-II broken-gap band alignment. Screening of the surface electric fields by the photogenerated carriers triggers the generation of a coherent acoustic phonon wavepacket, which propagates through the GaSb buffer layer. Since the probe pulse and the phonon wavepacket have different propagation velocities in GaSb, they go in and out of phase as they co-propagate. This gives rise to oscillations in probe reflectivity.

As discussed by Liu *et al.*, the period of oscillations can be expressed as $T = \lambda_{probe}/2C_s n_{ref}$, where C_s is the speed of sound and n_{ref} is the index of refraction of GaSb [14]. Using literature values for these parameters, and the wavelength of the probe, we calculate the period to be approximately 23–25 ps, which is in close agreement with the observed oscillations [figures 6 (*c*) and (*d*)]. High Mn doping in III–V DMSs produces larger surface electric fields, more efficiently generating phonon wavepackets. It is also worth pointing out that InMnAs/GaSb is more efficient for coherent phonon generation, in comparison to InGaMnAs/InGaAs, which can be also understood as a result of larger surface band bending in InMnAs.

We reemphasize the interesting situation in the first several picoseconds. The spontaneous symmetry breaking from the ferromagnetic order of Mn-spins, 'stimulated' symmetry breaking due to optical orientation of carrier-spins, and the mutual interaction between the two subsystems via $p-d$ coupling, coexist. This gives rise to the transient carrier-enhanced exchange coupling between Mn ions, a process which occurs with a characteristic time $\tau_{p-d} \sim \hbar/E_{p-d} = 4$ fs, where E_{p-d} is the $p-d$ exchange energy (conventionally denoted by $N_0\beta$ in DMS literature and ~ -1.0 eV in InMnAs [15]). We believe that this is at the core of the observed photoinduced softening. Two scenarios can be invoked based on different magnetization reversal mechanisms. One possible scenario is in terms of domain walls. Namely, an increase of $p-d$ exchange coupling breaks the original balance between the exchange energy and the anisotropy energy (the latter was found to be independent of carrier density [16]). The dominance of the former results in a decrease in domain wall energy, which results in the reduction of the magnetic field required to achieve magnetization reversal, i.e. coercivity is decreased. Another possible mechanism involves the magnetic rotation of single-domain particles known as magnetic polarons [17]. In an assembly of such particles, the interaction field among the particles is opposite to the particle magnetization and thus helps to reverse the particles. This gives rise to a reduction of the coercive field needed for magnetization reversal compared with that of a single particle. The size of the interaction field can be expressed as $ApM(p)$, where A, p, and $M(p)$ are the proportionality constant, the packing fraction, and single particle magnetization, respectively [18]. A large enhancement of the exchange coupling leads to the enlargement of magnetic polarons and thus increases the packing fraction p and single particle magnetization $M(p)$. This increases the interaction field and reduces the coercive force. In both cases, as soon as the transient photogenerated carriers are gone, the original value of the coercivity field is recovered. This is consistent with the notion that the extremely short-lived photogenerated carriers are the cause of ultrafast photoinduced softening.

5. Conclusions

In summary, we have identified a variety of ultrafast optical processes of charge, spin, phonons, and magnetic order in ferromagnetic InMnAs and InGaMnAs using two-colour time-resolved MOKE and reflectivity techniques. An ultrashort carrier charge/spin lifetime (~2 ps) and multi-level charge carrier decay dynamics were observed, which can be attributed to carrier trapping by mid-gap states due to low temperature MBE growth. We demonstrate *ultrafast photo-induced softening* in a single InMnAs/GaSb heterostructure, which constitutes

femtosecond control of ferromagnetic order in semiconductors. Photogenerated transient carriers significantly *decrease* the coercivity while sustaining the saturation magnetization. The transient softening persists only during the free carrier lifetime (~2 ps). Our novel observation, being non-thermal, is distinct from other known ultrafast processes of ferromagnetic order. Finally, large oscillations appearing in the differential reflectivity signal at long time delays are due to the coherent generation of acoustic phonon wavepackets in ferromagnetic semiconductors.

Acknowledgments

We thank Xiangfeng Wang for technical help and Yusuke Hashimoto for useful discussions. This work was supported by DARPA through MDA972-00-1-0034 and NSF through DMR-0134058 (CAREER), DMR-0325474 (ITR), and INT-0221704.

References

[1] For a review, see, e.g. ZHANG, G., HÜBNER, W., BEAUREPAIRE, E., and BIGOT, J.-Y., 2002, *Spin Dynamics in Confined Magnetic Structures I*, edited by B. Hillebrands and K. Ounadjela (Berlin: Springer), pp. 245–288.
[2] SEGRE, G. P., *et al*., 2002, *Phys. Rev. Lett*., **88,** 137001; GEDIK, N., *et al*., 2003, *Science*, **300,** 1410.
[3] KAINDL, R., *et al*., 2000, *Science*, **287,** 470.
[4] BEAUREPAIRE, E., MERLE, J.-C., DAUNOIS, A., and BIGOT, J.-Y., 1996, *Phys. Rev. Lett*., **76,** 4250.
[5] MUNEKATA, H., OHNO, H., VON MOLNAR, S., SEGMULLER, A., CHANG, L. L., and ESAKI, L., 1989, *Phys. Rev. Lett*., **63,** 1849; OHNO, H., MUNEKATA, H., PENNEY, T., VON MOLNAR, S., and CHANG, L. L., 1992, *ibid*., **68,** 2664.
[6] OHNO, H., SHEN, A., MATSUKURA, F., OIWA, A., ENDO, A., KATSUMOTO, S., and IYE, Y., 1996, *Appl. Phys. Lett*., **69,** 363.
[7] ORITZ, V., *et al*., 2002, *Appl. Phys. Lett*., **80,** 2505; KROTKUS, A., *et al*., 1939, *Appl. Phys. Lett*., **66,** 1939; GUPTA, S., *et al*., 1990, *Appl. Phys. Lett*., **57,** 1543.
[8] OHNO, H., CHIBA, D., MATSUKURA, F., OMIYA, T., ABE, E., DIETL, T., OHNO, Y., and OHTANI, K., 2000, *Nature*, **408,** 944.
[9] KOSHIHARA, S., OIWA, A., HIRASAWA, M., KATSUMOTO, S., IYE, Y., URANO, C., TAKAGI, H., and MUNEKATA, H., 1997, *Phys. Rev. Lett*., **78,** 4617.
[10] WANG, J., KHODAPARAST, G. A., KONO, J., SLUPINSKI, T., OIWA, A., and MUNEKATA, H., 2003, *J. Superconductivity*, **16,** 373; WANG, J., KHODAPARAST, G. A., KONO, J., SLUPINSKI, T., OIWA, A., and MUNEKATA, H., 2003, *Physica* E, **20,** 412.
[11] SLUPINSKI, T., OIWA, A., YANAGI, S., and MUNEKATA, H., 2002, *J. Cryst. Growth*, **237–239,** 1326.
[12] KUROIWA, T., YASUDA, T., MATSUKURA, F., SHEN, A., OHNO, Y., SEGAWA, Y., and OHNO, H., 1998, *Electron. Lett*., **190,** 34.
[13] ELLIOTT, R. J., 1954, *Phys. Rev*., **96,** 266.
[14] LIU, R., KIM, C. S., SANDERS, G. D., STANTON, C. J., YAHNG, J. S., JHO, Y. D., YEE, K. J., OH, E., and KIM, D. S., cond-mat/0310654.
[15] ZUDOV, M. A., KONO, J., MATSUDA, Y. H., IKAIDA, T., MIURA, N., MUNEKATA, H., SANDERS, G. D., SUN, Y., and STANTON, C. J., 2002, *Phys. Rev*. B, **66,** 161307.
[16] OIWA, A., SLUPINSKI, T., and MUNEKATA, H., 2001, *Appl. Phys. Lett*., **78,** 518.
[17] MUNEKATA, H., OIWA, A., and SLUPINSKI, T., 2002, *Physica* E, **13,** 516.
[18] ELDRIDGE, D. F., 1961, *J. Appl. Phys*., **32,** 247S.